Differentiating Between Alzheimer's Disease and Frontotemporal Dementia Based on the Resting-State Multilayer EEG Network

Yajing Si, Runyang He, Lin Jiang, Dezhong Yao, Hongxing Zhang, Peng Xu, *Member, IEEE*, Xuntai Ma, Liang Yu, and Fali Li

***Abstract*— Frontotemporal dementia (FTD) is frequently misdiagnosed as Alzheimer's disease (AD) due to similar clinical symptoms. In this study, we constructed frequency-based multilayer resting-state electroencephalogram (EEG) networks and extracted representative network features to improve the differentiation between AD and FTD. When compared with healthy controls (HC), AD showed primarily stronger delta-alpha cross-couplings and weaker theta-sigma cross-couplings. Notably, when comparing the AD and FTD groups, we found that the AD exhibited stronger delta-alpha and delta-beta connectivity than the FTD. Thereafter, by extracting the representative network features and then applying these features in the classification between AD and FTD, an accuracy of 81.1% was achieved. Finally, a multivariable linear regressive model was built, based on the differential topologies, and then adopted to predict the scores of the Mini-Mental State Examination (MMSE) scale. Accordingly, the predicted and actual measured scores were indeed significantly correlated with each other ($r = 0.274$, $p = 0.036$). These findings consistently suggest that frequency-based multilayer resting-state networks can be utilized for classifying AD and FTD and have potential applications for clinical diagnosis.**

***Index Terms*— Alzheimer's disease, Frontotemporal dementia, classification, resting-state multilayer network.**

I. Introduction

THE prevalence of Alzheimer's disease (AD) is rapidly increasing worldwide, with no approved and effective disease-modifying treatment available, significantly impacting the daily functioning and quality of life for patients [1]. AD is the most common form of dementia, characterized by cognitive impairments in affected individuals that remains poorly understood [2]. Frontotemporal dementia (FTD), often misdiagnosed as AD due to similar clinical symptoms, such as behavioral changes, executive dysfunction, language difficulties, and motor impairments, represents another prevalent form of dementia that poses significant safety risks for affected individuals [3]. Decision-making abilities related to medication management and meal preparation among individuals with dementia carry potential risks leading to severe consequences [4]. Therefore, accurate diagnosis of AD from FTD, along with appropriate symptomatic treatment, play a crucial role in addressing the needs of affected individuals.

Patients with FTD typically exhibit a more rapid decline in cognitive function, as well as shorter survival rates from the time of initial diagnosis, compared to individuals with AD. These underscore the importance of providing timely and accurate diagnoses, along with appropriate treatment interventions [5]. Previous research utilizing structural imaging has examined episodic memory, grammatical comprehension, naming abilities, and the relationship between self-appraisal and grey matter density in FTD and AD patients. That is, individuals with FTD demonstrated poor self-appraisal across all cognitive tasks, while those with AD exhibited reduced grey matter density in the subgenual cingulate region [6]. Meta-cognitive assessment studies have also aimed to identify cognitive deficits specific to the two types of dementia. Notably, metacognitive assessments have made significant progress in exploring the awareness levels across AD patients [7]. Furthermore, compared to AD patients, those with FTD displayed greater monitoring disorders and were less likely to utilize work experience for subsequent improvement or accuracy enhancement of monitoring judgments [4]. This supports the utility of metacognition measures as a means of distinguishing AD and FTD. However, it is important to acknowledge certain limitations associated with these methods, such as their costliness, time-consuming nature, and subjectivity. And more importantly, there is currently limited neural evidence available for effectively differentiating between AD and FTD.

In essence, during the resting state, our brain is still activated and characterized by a specific brain network mode [8], which has been widely clarified to correlate with brain

Manuscript received 11 August 2023; revised 7 October 2023; accepted 29 October 2023. Date of publication 3 November 2023; date of current version 16 November 2023. This work was supported in part by the China Postdoctoral Science Foundation under Grant 2021M700701, in part by the National Natural Science Foundation of China under Grant 62103085 and Grant U19A2082, in part by the STI 2030-Major Projects under Grant 2022ZD0211400 and Grant 2022ZD0208500, in part by the Key R&D Projects of Science and Technology Department of Sichuan Province under Grant 2023YFS0324 and Grant 2023YFS0080, in part by the Research Project in Sichuan Medical and Health Care Promotion Institute under Grant KY2022SJ0035, and in part by the Scientific Research Foundation of Sichuan Provincial People's Hospital under Grant 2021LY21. *(Yajing Si and Runyang He contributed equally to this work.) (Corresponding authors: Peng Xu; Xuntai Ma; Liang Yu; Fali Li.)*

This work involved human subjects in its research. Approval of all ethical and experimental procedures and protocols was granted by the Ethics Committee of University of Ioannina.

Please see the Acknowledgment section of this article for the author affiliations.

Digital Object Identifier 10.1109/TNSRE.2023.3329174

cognition [9]. The resting-state network efficiently characterizes the allocation of brain resources and aids in distinguishing patients from healthy controls (HC) clinically [10], [11]. For instance, by adopting the developed convolutional neural network model to classify individuals with Parkinson's disease and HC, based on their resting-state EEG, an accuracy of 99.2% was achieved [12]. As for AD, previous studies reported an accuracy of 77% in classifying AD from matched elderly HC [11], based on the resting-state eyes-closed EEG rhythms. Compared to elderly HC, those with AD have been characterized by low power in the posterior alpha rhythm as well as high power in theta and delta rhythms [13]. EEG rhythms are important features of collective behavior among human brain neuronal populations and are closely related to cognition. Furthermore, EEG is well-tolerated by patients, unaffected by individual anxiety levels, and can be repeated over time [14]. In this study, we hypothesized that AD and FTD may present distinct frequency-based brain networks in resting-state EEG that also may be neural markers to differentiate between the two patient groups. Thus, the current study aims to develop a frequency-based multilayer network (FMN) framework for effectively differentiating AD and FTD, based on the resting-state EEG. First, we developed the FMN to represent the resting-state brain activity of all patients and controls, in which the relevant bands were defined within delta (0.5-5 Hz), theta 4-8 Hz), alpha 8-12.5 Hz), sigma (12.5-15.5 Hz), and beta (15.5-30 Hz). Subsequently, FMN features were retrieved from the resting-state EEG networks of all participants and were then employed in distinct classifying models to accomplish the classification between AD and FTD.

II. Methods

A. Dataset

G*Power 3.1 software was utilized to calculate the sample size of the used dataset. Using one-way ANOVA as a statistical method, the parameters were set as effect size $f = 0.45$, $\alpha = 0.05$, 1-$\beta = 0.95$, and number of groups = 3, which showed that the total sample size should be at least 81. Herein, an open dataset (https://openneuro.org/datasets/ds004504/versions/1.0.2) comprising eye-closed resting-state EEG datasets was utilized to conduct a specific analysis of distinguishing between AD and FTD, in which 36 participants (24 females, 66.4 ± 7.9 years old) were diagnosed with AD, 23 participants (9 females, 63.6 ± 8.2 years old) were diagnosed with FTD, and the remaining 29 (11 females, 67.9 ± 5.4 years old) served as HC. The cognitive and neuropsychological status was evaluated using the internationally recognized Mini-Mental State Examination (MMSE), which yields scores ranging from 0 to 30, and lower MMSE scores indicate more pronounced cognitive declines. The average MMSE score for individuals with AD was found to be 17.75 ± 4.5, while for FTD, it was recorded as 22.17 ± 8.22, and the HC consistently exhibited an MMSE score of 30. The duration of the disease was measured in months, with a median value of 25 and an interquartile range (IQR) of 24 -28.5 months. No comorbidities related to dementia were reported within the AD group.

B. EEG Recording

The recordings were obtained from the 2nd Department of Neurology at AHEPA General Hospital in Thessaloniki by a team of experienced neurologists. And a Nihon Kohden EEG 2100 clinical device with 19 electrodes (Fp1, Fp2, F7, F3, Fz, F4, F8, T3, C3, Cz, C4, T4, T5, P3, Pz, P4, T6, O1, and O2) was utilized. Each recording followed the clinical protocol with participants seated and their eyes closed. Prior to the recording session, the impedance per electrode was maintained below 5 kΩ, and the sampling rate was set at 500 Hz. The recording montages consisted of anterior-posterior bipolar and referential montages using Cz as the common reference. The received recordings adhered to specific amplifier parameters: sensitivity set at 10uV/mm, time constant at 0.3 s, and high-frequency filter set at 70 Hz. Each recording lasted 13.5 minutes for the AD group (a range of [5.1, 21.3] min), 12 minutes for the FTD group (a range of [7.9, 16.9] min), and 13.8 for the HC group (a range of [12.5, 16.5] min). In total, 485.5 minutes of AD, 276.5 minutes of FTD, and 402 minutes of HC recordings were obtained.

C. Resting-State EEG Preprocessing

The preprocessing pipeline of the resting-state EEG signals was as follows. A Butterworth band-pass filter 0.5-45 Hz was adopted, and the signals were re-referenced to A1-A2. Then, the Artifact Subspace Reconstruction routine (ASR) was applied to correct an EEG artifact, removing bad data periods that exceeded the maximum acceptable 0.5-second window standard deviation of 17. Next, the Independent Component Analysis (ICA) was conducted to classify "eye artifacts" or "jaw artifacts" which were automatically rejected. 5-s data segmentation and artifact trial removal (± 150 μV serve as threshold) was also applied herein. After preprocessing, the number of remaining segments (trials) was 146.56 ± 34.05 for the AD group, 128.65 ± 39.46 for the FTD group, and 149.70 ± 16.56 for the HC group.

D. Resting-State Multilayer Network Analysis

Analysis procedures for resting-state EEG data were presented in Fig.1. First, we constructed resting-state multilayer networks in five bands (i.e., delta, theta, alpha, sigma, and beta) based on 5-second-long preprocessed segments. And for all participants, these networks were constructed based on the intra- and cross-frequency couplings, in which the corresponding measurements of inter-electrode couplings were accomplished by adopting phase-locking value (PLV) [15]. The PLV is skilled in capturing the non-linear phase synchronization, and relying on this, PLV effectively quantifies the phase synchronization between two brain regions [16], as well as evaluates the association between brain network linkage and cognition [15], [17], [18]. Therefore, following the protocols adopted in the above studies, the PLV was also used to estimate the phase-synchronization and then construct the network. The Hilbert transform (HT) was employed to establish the analytical signal $H(t)$, which allowed us to evaluate the instantaneous phases $\varphi_x(t)$ and $\varphi_y(t)$ of two given time series $x(t)$ and $y(t)$,

$$\begin{cases} H_x(t) = x(t) + iHT_x(t) \\ H_y(t) = y(t) + iHT_y(t) \end{cases} \quad (1)$$

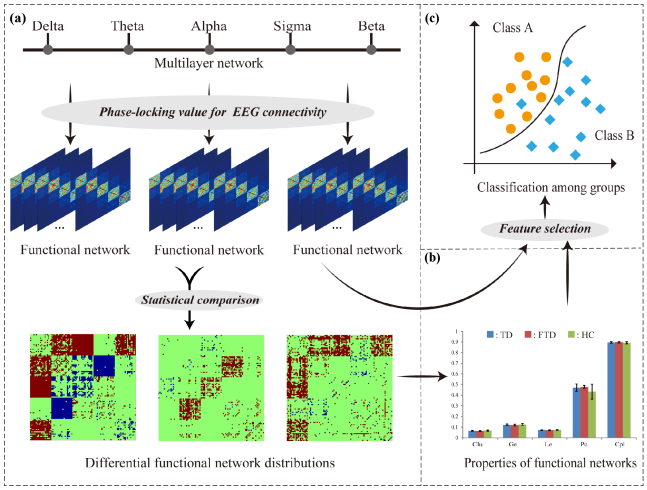

Fig. 1. Analysis procedures for resting-state EEG data. (a) Resting-state multilayer brain network construction, (b) properties of functional network estimation, and (c) feature section and classification.

where $HT_x(t)$ *and* $HT_y(t)$ are the HT of the time series, $x(t)$ and $y(t)$, which are formulated as:

$$\begin{cases} HT_x(t) = \dfrac{1}{\pi} P.V. \displaystyle\int_{-\infty}^{\infty} \dfrac{x(t')}{t-t'} dt' \\ HT_y(t) = \dfrac{1}{\pi} P.V. \displaystyle\int_{-\infty}^{\infty} \dfrac{y(t')}{t-t'} dt' \end{cases} \tag{2}$$

where the *P.V.* represents the Cauchy principal value. The analytical signal phases of $\varphi_x(t)$ and $\varphi_y(t)$ are as follows,

$$\begin{cases} \varphi_x = \arctan \dfrac{HT_x(t)}{x(t)} \\ \varphi_y = \arctan \dfrac{HT_y(t)}{y(t)} \end{cases} \tag{3}$$

Here, PLV can be expressed as follows,

$$w^{plv} = \left| \frac{1}{N} \sum_{j=0}^{N-1} e^{i(\varphi_x(j\Delta t) - \varphi_y(j\Delta t))} \right| \tag{4}$$

where w^{plv} is the connection weight estimated by PLV, t is the time point, Δt denotes the sampling period, j denotes the j-th sample point and N is the sample number of each signal.

For each participant, a weighted adjacency matrix, with a dimension of 19 × 19, was first computed per segment per band, and across all segments, the matrices were then averaged to obtain a final matrix per band. The brain network was constructed by assigning the w^{PLV} (weighted phase locking value) as the corresponding edge between each pair of electrodes. To quantitatively assess the characteristics of the PLV network, multiple metrics including clustering coefficient (*Clu*), local efficiency (*Le*), global efficiency (*Ge*), characteristic path length (L), and participation coefficient (*Pc*) were measured. They are formulated as follows,

$$Clu = \frac{1}{N} \sum_{i \in \theta} \frac{\sum_{j,l \in \theta} (w_{ij} w_{il} w_{jj})^{1/3}}{\sum_{j \in w_{ij}} (\sum_{j \in \theta} w_{ij} - 1)} \tag{5}$$

$$L_e = \frac{1}{N} \sum_{i \in \theta} \frac{\sum_{j,l \in \theta, j \neq i} (w_{ij} w_{il} [d_{jl}(\theta_i)]^{-1})^{1/3}}{\sum_{j \in \theta} w_{ij} (\sum_{j \in \theta} w_{ij} - 1)} \tag{6}$$

$$G_e = \frac{1}{N} \sum_{i \in \theta} \frac{\sum_{j \in \theta, j \neq i} d_{ij}^{-1}}{N-1} \tag{7}$$

$$L = \frac{1}{N} \sum_{i \in \theta} L_i = \frac{1}{N} \sum_{i \in \theta} \frac{\sum_{j \in \theta, j \neq i} d_{ij}}{N-1} \tag{8}$$

$$Pc = \frac{1}{N} \sum_{i \in \theta} Pc_i = \frac{1}{N} \sum_{i \in \theta} (1 - \sum_{m} (\frac{d_i^m}{d_i})^2) \tag{9}$$

where w_{ij} is the coherence value between i and j, N represents the node number, and θ is the set of all nodes. The SPSS statistics 17.0 was utilized in the current work to explore the network differences among AD, FTD, and HC.

E. Feature Selection Analysis

In the present study, three categories were employed to achieve feature extraction: intra-frequency coupling, cross-frequency coupling, and graph features. And a total of 4470 metrics were obtained for subsequent investigation. Concretely, cross-frequency phase-to-phase synchronization, a form of cross-frequency coupling, was used to define the balance between information integration and segregation. Traditional functional connectivity within each band was adopted as an intra-frequency feature. Feature selection plays a crucial role in determining the output by automatically identifying the most relevant characteristics. Statistical tests were applied to select features that exhibited the strongest relationship with the output variable, and herein, the analysis of variance (ANOVA) F-value statistics was employed for feature selection.

F. Classification Among the Three Groups

The classification performances of 12 machine learning (ML) algorithms, including k-nearest neighbor (KNN) and Gaussian Naive Bayes (GNB), support vector machine (SVM), random forest (RF), gradient boosting (GB), decision tree (DT), extra tree (ET), light gradient boosting machine (light GBM), cat boost, Ada boost, extreme gradient boosting (XGBoost), and ridge classifier, were evaluated on three classification problems: AD vs. FTD, AD vs. HC, and FTD vs. HC. Additionally, for each ML algorithm, a 5-fold cross-validation testing was employed, in which, the whole dataset is divided into five roughly equal folds. And during each iteration, four folds are used as the training set while the remaining fold is used as the testing set. The model is trained on the training set and evaluated on the testing set. This process is repeated five times with each fold serving as the testing set once.

Multiple metrics, including accuracy, precision, recall, F1 score and AUC score, that evaluate the classification performances were calculated for each classification case. Concretely, assuming AUC score represents the area under ROC curve which plots true positive rate against false positive rate, and the formulas defining other metrics are as follows:

$$Accuracy = \frac{TP + TN}{TP + TN + FP + FN} \tag{10}$$

$$Precision = \frac{TP}{TP + FP} \tag{11}$$

$$Recall = \frac{TP}{TP + FN} \tag{12}$$

$$F1score = \frac{2 \times Precision \times Recall}{Precison + Recall} \tag{13}$$

where *TP* indicates the positive group of being correctly classified, *TN* indicates the negative group of being correctly classified, *FP* indicates the positive group of being wrongly classified, and *FN* indicates the negative group of being wrongly classified.

G. The MMSE Prediction Based on Multiple Linear Regression Model

Eventually, to achieve the prediction of individual MMSE scores, by utilizing resting-state PLV and five network properties as variable, the multiple linear regression model was constructed. Thereinto, the key parameters of the multiple linear regression model comprise independent variables, dependent variable, and coefficients. Specifically, the dependent variable is the score on the Mini-Mental State Examination (MMSE), which serves as a measure of cognitive function. The independent variables consist of 45 selected features chosen using the ANOVA F-value statistical method, primarily encompassing cross-frequency characteristics. These features primarily encompass cross-frequency characteristics. Each independent variable is associated with a coefficient that reflects its impact on the dependent variable, and related coefficients for each independent variable in the model are then estimated linearly accordingly. Herein, to accurately assess its predictive capacity, the leave-one-out cross-validation (LOOCV) strategy was employed [19], where every time one subject would be left out as the testing sample. Assuming N participants were involved, within each LOOCV iteration, N-1 samples were utilized for training while the remaining 1 sample was utilized for testing. After evaluating the regression coefficient for each variable, a prediction model was built based on current N-1 samples and further utilized to predict individual MMSE score in the test set. This process would be repeated N times until all samples served as testing set for one time. Thereafter, prediction performance was measured by calculating the correlation coefficient between actual and predicted MMSE scores through Pearson's correlation analysis, while root mean square error (RMSE) was calculated to measure prediction error,

$$RMSE = \sqrt{\frac{1}{N}\sum_{t=1}^{N}(X_t - Y_t)^2} \tag{14}$$

where N denotes the participant size. X and Y are the actual and predicted MMSE scores, respectively. Here, a smaller RMSE accounts for a better prediction.

III. Results

A. Differential Resting-State Networks in Five Bands

The within- and cross-frequency coupling differences in the resting-state networks among AD, FTD, and HC are displayed in Fig. 2. As illustrated, it can be observed that there were stronger delta-alpha couplings in the AD group compared to the HC group ($p < 0.05$, FDR corrected), while in terms of theta-sigma coupling, the HC group exhibited stronger cross-frequency linkages than the AD group. Regarding potential differences between HC and FTD, stronger linkages were found in the HC group for both intra-alpha and theta-sigma couplings. Furthermore, when comparing the two patient groups (AD vs. FTD), the AD demonstrated stronger values in delta-alpha and delta-beta coupling, compared to the FTD.

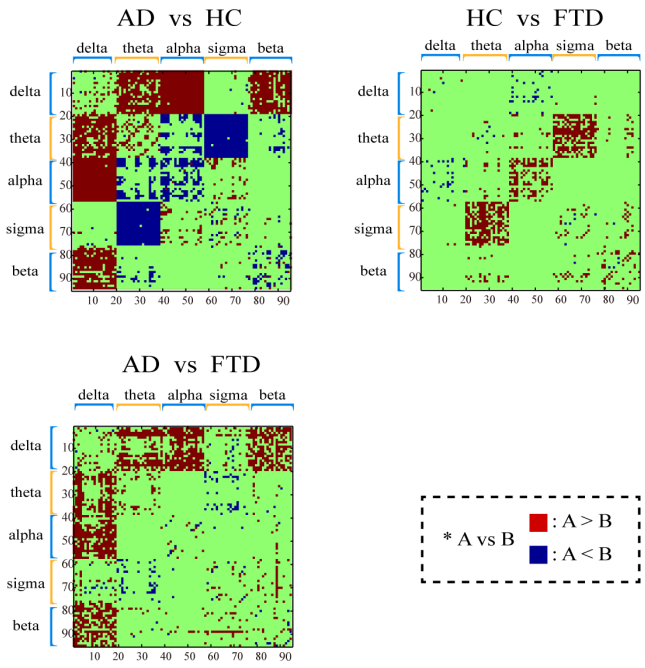

Fig. 2. Differential resting-state networks among AD, FTD, and HC within and across five bands. The red block denotes the stronger linkages in A than in B, and the blue block denotes the opposite.

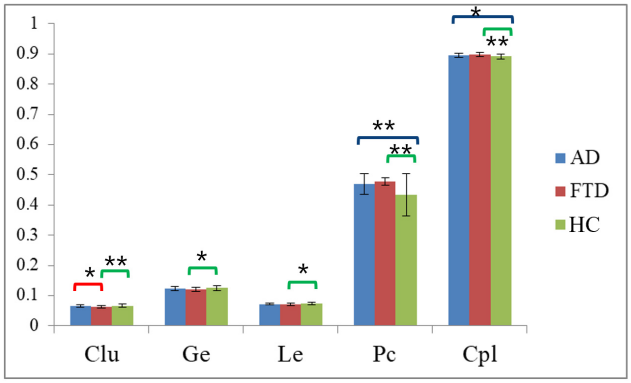

Fig. 3. Differences in network properties among AD, FTD, and HC. * represents p < 0.05; ** represents p < 0.01.

B. Resting-State Network Properties Difference Among AD, FTD, and HC

Based on the multilayer networks constructed by the intra- and cross-frequency coupling, for each participant, the corresponding resting-state network properties were then calculated. And any potential difference among the three groups was statistically investigated and presented in Fig. 3. From Fig. 3, it can be observed that compared to the FTD, the HC exhibited higher *Clu*, *Ge*, *Le,* and lower *Pc* and *Cpl* ($t = 2.754$, 2.252, 2.460, -2.908, and -2.765, respectively; $p < 0.05$). Additionally, the *Clu* of AD was higher than that of FTD ($t = 1.713$, $p < 0.05$), while both *Pc* and *Cpl* of AD were higher than those of HC (t= 2.726 and 1.961, respectively; $p < 0.05$).

C. Classification Among AD, FTD, and HC Based on Resting-State Multilayer Network Topologies and Properties

To improve classification performance and reduce computational complexity, the ANOVA F-value statistical method

TABLE I
CLASSIFICATION PERFORMANCE AMONG AD, FTD, AND HC BASED ON MULTILAYER RESTING-STATE NETWORKS

Model	Accuracy	Precision	Recall	F1 score	AUC score
GNB	0.811/0.862/ 0.847	0.712/0.823/ 0.870	0.810/0.900/ 0.867	0.789/0.860/ 0.844	0.901/0.907/ 0.907
ET	0.762/0.846/ 0.827	0.718/0.823/ 0.848	0.590/0.900/ 0.867	0.697/0.844/ 0.799	0.863/0.892/ 0.911
Light GBM	0.729/0.831/ 0.807	0.698/0.853/ 0.824	0.600/0.767/ 0.867	0.705/0.826/ 0.797	0.817/0.883/ 0.924
RF	0.711/0.862/ 0.847	0.693/0.823/ 0.870	0.640/0.900/ 0.867	0.709/0.860/ 0.819	0.871/0.880/ 0.915
Cat Boost	0.711/0.846/ 0.827	0.670/0.823/ 0.848	0.600/0.867/ 0.827	0.680/0.844/ 0.819	0.837/0.889/ 0.939
SVM	0.679/0.785/ 0.827	0.598/0.745/ 0.817	0.540/0.800/ 0.900	0.644/0.782/ 0.817	0.837/0.876/ 0.878
XG Boost	0.645/0.862/ 0.747	0.619/0.853/ 0.781	0.430/0.833/ 0.827	0.601/0.859/ 0.729	0.781/0.897/ 0.855
Ridge	0.612/0.800/ 0.825	0.467/0.772/ 0.837	0.280/0.800/ 0.867	0.514/0.797/ 0.817	0.818/0.866/ 0.875
Ada Boost	0.644/0.785/ 0.767	0.572/0.795/ 0.815	0.530/0.733/ 0.827	0.618/0.779/ 0.778	0.770/0.873/ 0.911
KNN	0.729/0.677/ 0.638	0.633/0.752/ 0.820	0.410/0.500/ 0.520	0.636/0.639/ 0.613	0.786/0.727/ 0.701
DT	0.608/0.723/ 0.711	0.463/0.760/ 0.731	0.430/0.700/ 0.633	0.561/0.780/ 0.647	0.525/0.746/ 0.737
GB	0.594/0.800/ 0.709	0.487/0.772/ 0.749	0.400/0.800/ 0.767	0.539/0.813/ 0.691	0.617/0.813/ 0.743

Note: The column values represent the classification indices of AD/FTD, AD/HC, and FTD/HC, respectively.

was used to select features. Herein, the classification algorithm used was GNB, and to ensure the most satisfying performance, varying numbers of features were selected to accomplish the classification of AD and FTD; after applying the ANOVA F-value statistical method, we found that the GBN classifier can obtain the highest accuracy when the number of features is 45. Based on multiple metrics of multilayer resting-state networks (i.e., within- and cross-frequency coupling and network properties), we further classified individuals into three groups: AD, FTD, and HC. A comprehensive approach was employed to select an appropriate ML model, in which all 4470 features were utilized as inputs for twelve ML methods. Thereafter, the classification results are listed in Table I, relying on selected features and a 5-fold cross-validation technique. Multiple measurements (i.e., accuracy, precision, recall, F1 score, and AUC score) were calculated to further evaluate the performance of these ML methods. Just as displayed in Table I, Naive Bayes achieved the best performance, with classification accuracies of 0.811/0.862/0.847, precisions of 0.712/0.823/0.870, recall rates of 0.810/0.900/0.867, F1 scores of 0.789/0.860/0844 and AUC scores of 0.901/0.907/0.907 among AD /FTD, AD /HC, and FTD /HC, respectively.

D. MMSE Prediction Based on Multilayer Resting-State Networks

Through the ANOVA, the difference in MMSE was analyzed among the three groups (i.e., AD, FTD, and HC), which did reveal significant differences ($F = 119.735$, $p < 0.001$). Concretely, the MMSE of AD (17.75 ± 4.50) was lower than that of FTD (22.17 ± 2.64), and the MMSE of FTD was lower than that of HC (30.00 ± 0.00). Given the observed differences in resting-state networks among AD, FTD, and HC, these features can thus potentially serve as features for predicting an individual's MMSE score. Fig. 4 illustrates the relationship between predicted and actual scores, where the X-axis represents the actual scores and the Y-axis represents the predicted scores. There is a Pearson's correlation coefficient of 0.274 ($p = 0.036$) between the predicted and actual MMSE scores, along with an RMSE of 8.03%.

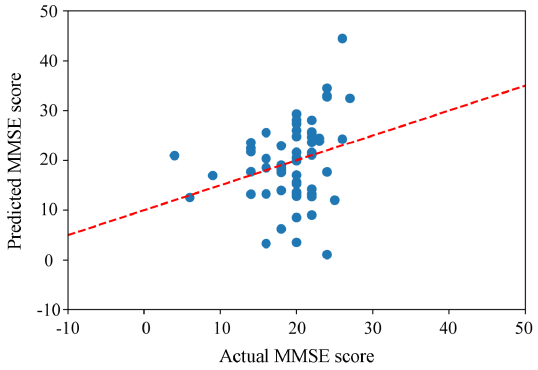

Fig. 4. The relationship between actual (X-axis) and predicted (Y-axis) MMSE scores. The blue-filled circles are the participants.

IV. DISCUSSION

The resting-state brain serves as a cornerstone for various cognitive tasks [20], including attention and cognition control [21], [22]. Abnormal activity in the resting brain is associated with clinical psychiatric disorders such as depression, attention deficit hyperactivity disorder, and anxiety [23]. In this study, we observed stronger delta-alpha couplings within the resting-state network in AD compared to HC. Previous studies have demonstrated that alpha activity is linked to individual behavioral performance [24], cognitive preparedness, and attentional arousal [25], [26]. And delta oscillation has also been found to correlate with human attention, reward prediction, and motivation during task performance [27], [28]. Furthermore, a previous study revealed increased spectral power and coherence analysis of delta activity in AD compared to HC [29]. Therefore, it can be inferred that AD patients exhibit hyperactivity within the delta-alpha bands due to a lack of task-related attention. This lack of concentration impairs their ability to complete tasks successfully. Importantly, our current findings indicate that patients with AD display stronger delta-alpha couplings compared to those with FTD. This suggests that enhanced synchronization within these bands may reflect an abnormal pre-configuration of related brain resources that are essential for human cognition tasks involving attentional arousal. Moreover, it may serve as a valuable index for differentiating between AD and FTD based on the frequency information derived from multilayer EEG networks.

During the frequency coupling analysis, our study found that the HC exhibited stronger theta-sigma couplings, compared to both AD and FTD. The theta band is strongly associated with memory encoding of concrete cognitive tasks [30], and modulation of memory-dependent theta activation is linked to EEG synchronization among a distributed network [31]. Our study further revealed that increased theta-sigma synchronization played an essential role in healthy individuals for preparing for subsequent cognitive tasks. This suggests

that theta-sigma synchronization forms a global EEG network among memory-related areas, contributing to the flexible formation of the global network. However, AD or FTD patients showed obvious memory loss and an inability to respond flexibly to daily life events. The properties result of multiple networks also confirmed this finding by showing higher *Clu*, *Ge*, *Le*, and lower *Pc* and *Cpl* corresponded with the HC, compared to patient groups, reflecting an increase in information processing efficiency of healthy brains [24]. Regarding differences between HC and FTD, we reported stronger resting-state network linkages in the alpha band for the HC as well. In general, the alpha band is thought to be associated with attentional arousal as well as cognitive preparedness [25] involving information processing speed, working memory, and inhibition [25], [32], [33]. Therefore, network activity in intra-alpha and theta-sigma bands may preconfigure crucial cognitive resources for subsequent events revealing the potential of the brain for efficiently processing information.

The EEG has become an effective diagnostic tool in most cases of dementia, including AD and FTD. Previous related classification studies have adopted ML methods to provide an insight for early dementia diagnosis, showing the accuracy of 78.5% for AD/HC with decision trees and 86.3% for FTD/HC with random forests [34], [35]. In the current study, based on the multilayer network features, including within- and cross-frequency coupling and network properties, an automated framework was further developed for classifying AD, FTD, and HC. Just as listed in Table I, Gaussian Naive Bayes (GNB) achieved the most satisfying performance in terms of accuracy, precision, and other indexes. It is noteworthy that GNB demonstrates significantly higher classification accuracy than other classification algorithms when it comes to accurately classifying AD and FTD. This indicates that GNB has better adaptability and classification capability in dealing with the specific features of these two diseases. Additionally, most input features conform to the normal distribution based on Shapiro-Wilk normality test ($p > 0.05$), which aligns with the assumption of GNB that the probability distribution of features follows a normal distribution. Therefore, compared to other algorithms, GNB is better able to describe the relationships between features, resulting in higher classification accuracy. Meanwhile, concerning the model complexity, the parameter estimation of GNB is relatively simple, that is, we only need to calculate the mean and variance of each category on each feature. Thus, its data processing speed is fast, and the process of training and prediction can be completed quickly. Additionally, other literature has also highlighted the advantages of GNB in early detection and classification of cancers [36], as well as monitoring human activity [37]. In fact, the differences in network topologies and properties coincided with those presented in Figs 2 and 3. In essence, frequency-based multilayer networks present good learning and generalization capabilities due to their simple modular structure that leads to parallel flexible brain architecture [38]. And further, these topological features have been utilized as effective classification indices for different cognitive conditions (e.g., emotion recognition) and clinical patients (e.g., psychogenic nonepileptic seizures and epilepsy) [17], [39], [40], [41]. Motivated by close relationships between resting-state indexes (i.e., topologies and properties) of the multilayer networks and individual MMSE scores, multiple linear regression analysis was performed to build a model for predicting their MMSE scores. The results depicted in Fig. 4 did exhibit clinical efficacy in predicting the mental status of patients based on our developed multiple linear regression model. In fact, the cognitive state of the subjects can be better reflected during their involvement in specific tasks. However, given this is a public-available dataset, the task EEG was not reported. Thus, based on resting-state EEG, the frequency-based multilayer networks were constructed, and related representative network features were extracted to differentiate between AD and FTD. In future studies, we would combine the cognitive tasks to conduct an in-depth analysis, to explore the mechanism underlying the variability between AD and FTD, thus promoting the transference of these cognitive findings to daily diagnoses clinically. Another possible limitation of the current study was that the sample size was constant in this open dataset, and the sample size indeed influenced the findings to some degree. In our future work, more subjects will be considered for the related clinical studies.

In conclusion, our findings clarified the crucial role of a frequency-based multilayer resting-state network in differentiating AD and FTD. And by utilizing related network topologies and properties as variables, the proposed framework can reliably predict an individual's cognitive and neuropsychological state. Collectively, these findings deepen our understanding of AD and FTD from the perspective of resting-state multilayer networks and may offer a potential physiological biomarker for distinguishing AD and FTD in clinical settings.

Acknowledgment

Yajing Si is with the MOE Key Laboratory for Neuroinformation, the Center for Information in BioMedicine, the School of Life Science and Technology, and the Clinical Hospital of Chengdu Brain Science Institute, University of Electronic Science and Technology of China, Chengdu 610054, China, and also with the School of Psychology, Xinxiang Medical University, Xinxiang 453003, China.

Runyang He and Lin Jiang are with the MOE Key Laboratory for Neuroinformation, the Center for Information in BioMedicine, the School of Life Science and Technology, and the Clinical Hospital of Chengdu Brain Science Institute, University of Electronic Science and Technology of China, Chengdu 610054, China.

Dezhong Yao is with the MOE Key Laboratory for Neuroinformation, the Center for Information in BioMedicine, the School of Life Science and Technology, and the Clinical Hospital of Chengdu Brain Science Institute, University of Electronic Science and Technology of China, Chengdu 610054, China, also with the Research Unit of NeuroInformation, Chinese Academy of Medical Sciences, Chengdu 611731, China, and also with the School of Electrical Engineering, Zhengzhou University, Zhengzhou 450001, China.

Hongxing Zhang is with the School of Psychology, Xinxiang Medical University, Xinxiang 453003, China.

Peng Xu is with the MOE Key Laboratory for Neuroinformation, the Center for Information in BioMedicine, the School of Life Science and Technology, and the Clinical Hospital of Chengdu Brain Science Institute, University of Electronic Science and Technology of China, Chengdu 610054, China, also with the Research Unit of NeuroInformation, Chinese Academy of Medical Sciences, Chengdu 611731, China, also with the Radiation Oncology Key Laboratory of Sichuan Province, Chengdu 610042, China, and also with the Rehabilitation Center, Qilu Hospital of Shandong University, Jinan 250062, China (e-mail: xupeng@uestc.edu.cn).

Xuntai Ma is with the Clinical Medical College of Chengdu Medical College, Chengdu 610500, China, and also with The First Affiliated Hospital of Chengdu Medical College, Chengdu 610599, China (e-mail: maxuntai2002@126.com).

Liang Yu is with the Department of Neurology, Sichuan Provincial People's Hospital, University of Electronic Science and Technology of China, Chengdu 610054, China, and also with the Chinese Academy of Sciences Sichuan Translational Medicine Research Hospital, Chengdu 610041, China (e-mail: 18981838653@163.com).

Fali Li is with the MOE Key Laboratory for Neuroinformation, the Center for Information in BioMedicine, the School of Life Science and Technology, and the Clinical Hospital of Chengdu Brain Science Institute, University of Electronic Science and Technology of China, Chengdu 610054, China, also with the Research Unit of NeuroInformation, Chinese Academy of Medical Sciences, Chengdu 611731, China, and also with the Department of Electrical and Computer Engineering, Faculty of Science and Technology, University of Macau, Macao, China (e-mail: fali.li@uestc.edu.cn).

REFERENCES

[1] B. Michael and M. Ellul, "Global, regional, and national burden of neurological disorders, 1990–2016: A systematic analysis for the Global Burden of Disease Study 2016," *Lancet Neurol.*, vol. 18, pp. 459–480, May 2019.

[2] S. Cosentino and Y. Stern, "Metacognitive theory and assessment in dementia: Do we recognize our areas of weakness?" *J. Int. Neuropsychological Soc.*, vol. 11, no. 7, pp. 909–910, Nov. 2005.

[3] N. T. Olney, S. Spina, and B. L. Miller, "Frontotemporal dementia," *Neurologic Clinics*, vol. 35, pp. 339–374, May 2017.

[4] S. J. DeLozier and D. Davalos, "A systematic review of metacognitive differences between Alzheimer's disease and frontotemporal dementia," *Amer. J. Alzheimer's Disease Dementias*, vol. 31, pp. 381–388, Aug. 2016.

[5] K. Rascovsky et al., "Sensitivity of revised diagnostic criteria for the behavioural variant of frontotemporal dementia," *Brain*, vol. 134, pp. 2456–2477, Sep. 2011.

[6] L. Massimo et al., "Self-appraisal in behavioural variant frontotemporal degeneration," *J. Neurol., Neurosurgery Psychiatry*, vol. 84, no. 2, pp. 148–153, Feb. 2013.

[7] S. Cosentino, "Metacognition in Alzheimer's disease," in *The Cognitive Neuroscience of Metacognition*. Heidelberg, Germany: Springer, 2014, pp. 389–407.

[8] M. E. Raichle and A. Z. Snyder, "A default mode of brain function: A brief history of an evolving idea," *NeuroImage*, vol. 37, no. 4, pp. 1083–1090, Oct. 2007.

[9] Y. Huang et al., "Vigilant attention mediates the association between resting EEG alpha oscillations and word learning ability," *NeuroImage*, vol. 281, Nov. 2023, Art. no. 120369.

[10] J. Shao, F. Zhang, C. Chen, Y. Wang, Q. Wang, and J. Zhou, "Brain network for exploring the change of brain neurotransmitter 5-hydroxytryptamine of autism children by resting-state EEG," *Comput. Math. Methods Med.*, vol. 2022, pp. 1–8, Apr. 2022.

[11] A. I. Triggiani et al., "Classification of healthy subjects and Alzheimer's disease patients with dementia from cortical sources of resting state EEG rhythms: A study using artificial neural networks," *Frontiers Neurosci.*, vol. 10, p. 604, Jan. 2017.

[12] S. Lee et al., "A convolutional-recurrent neural network approach to resting-state EEG classification in Parkinson's disease," *J. Neurosci. Methods*, vol. 361, Sep. 2021, Art. no. 109282.

[13] J. Jeong, "EEG dynamics in patients with Alzheimer's disease," *Clin. Neurophysiol.*, vol. 115, no. 7, pp. 1490–1505, Jul. 2004.

[14] C. Babiloni et al., "Brain neural synchronization and functional coupling in Alzheimer's disease as revealed by resting state EEG rhythms," *Int. J. Psychophysiol.*, vol. 103, pp. 88–102, May 2016.

[15] F. Li et al., "Differentiation of schizophrenia by combining the spatial EEG brain network patterns of rest and task P300," *IEEE Trans. Neural Syst. Rehabil. Eng.*, vol. 27, no. 4, pp. 594–602, Apr. 2019.

[16] V. Sakkalis, "Review of advanced techniques for the estimation of brain connectivity measured with EEG/MEG," *Comput. Biol. Med.*, vol. 41, no. 12, pp. 1110–1117, Dec. 2011.

[17] P. Li et al., "EEG based emotion recognition by combining functional connectivity network and local activations," *IEEE Trans. Biomed. Eng.*, vol. 66, no. 10, pp. 2869–2881, Oct. 2019.

[18] C. Yi et al., "A novel method for constructing EEG large-scale cortical dynamical functional network connectivity (dFNC): WTCS," *IEEE Trans. Cybern.*, vol. 52, no. 12, pp. 12869–12881, Dec. 2022.

[19] Y. Tian et al., "Spectral entropy can predict changes of working memory performance reduced by short-time training in the delayed-match-to-sample task," *Frontiers Hum. Neurosci.*, vol. 11, p. 437, Aug. 2017.

[20] Y. Zhang, P. Xu, D. Guo, and D. Yao, "Prediction of SSVEP-based BCI performance by the resting-state EEG network," *J. Neural Eng.*, vol. 10, no. 6, Dec. 2013, Art. no. 066017.

[21] F. Li et al., "Relationships between the resting-state network and the P3: Evidence from a scalp EEG study," *Sci. Rep.*, vol. 5, no. 1, p. 15129, Oct. 2015.

[22] R. Zhang et al., "Efficient resting-state EEG network facilitates motor imagery performance," *J. Neural Eng.*, vol. 12, no. 6, Dec. 2015, Art. no. 066024.

[23] J. J. Newson and T. C. Thiagarajan, "EEG frequency bands in psychiatric disorders: A review of resting state studies," *Frontiers Human Neurosci.*, vol. 12, p. 521, Jan. 2019.

[24] Y. Si et al., "Predicting individual decision-making responses based on the functional connectivity of resting-state EEG," *J. Neural Eng.*, vol. 16, no. 6, Oct. 2019, Art. no. 066025.

[25] W. Klimesch, "Alpha-band oscillations, attention, and controlled access to stored information," *Trends Cognit. Sci.*, vol. 16, no. 12, pp. 606–617, Dec. 2012.

[26] E. Angelakis, J. F. Lubar, S. Stathopoulou, and J. Kounios, "Peak alpha frequency: An electroencephalographic measure of cognitive preparedness," *Clin. Neurophysiol.*, vol. 115, no. 4, pp. 887–897, Apr. 2004.

[27] C. S. Gilmore, S. M. Malone, E. M. Bernat, and W. G. Iacono, "Relationship between the P3 event-related potential, its associated time-frequency components, and externalizing psychopathology," *Psychophysiology*, vol. 47, no. 1, pp. 123–132, Jan. 2010.

[28] G. G. Knyazev, "EEG delta oscillations as a correlate of basic homeostatic and motivational processes," *Neurosci. Biobehavioral Rev.*, vol. 36, no. 1, pp. 677–695, Jan. 2012.

[29] A. H. Meghdadi et al., "Resting state EEG biomarkers of cognitive decline associated with Alzheimer's disease and mild cognitive impairment," *PLoS ONE*, vol. 16, no. 2, Feb. 2021, Art. no. e0244180.

[30] G. Sammer et al., "Relationship between regional hemodynamic activity and simultaneously recorded EEG-theta associated with mental arithmetic-induced workload," *Human Brain Mapping*, vol. 28, no. 8, pp. 793–803, Aug. 2007.

[31] N. Sato, "Fast entrainment of human electroencephalogram to a theta-band photic flicker during successful memory encoding," *Frontiers Human Neurosci.*, vol. 7, p. 208, May 2013.

[32] W. Klimesch, "Memory processes, brain oscillations and EEG synchronization," *Int. J. Psychophysiology*, vol. 24, nos. 1–2, pp. 61–100, Nov. 1996.

[33] C. Richard Clark et al., "Spontaneous alpha peak frequency predicts working memory performance across the age span," *Int. J. Psychophysiol.*, vol. 53, no. 1, pp. 1–9, Jun. 2004.

[34] A. Miltiadous et al., "Alzheimer's disease and frontotemporal dementia: A robust classification method of EEG signals and a comparison of validation methods," *Diagnostics*, vol. 11, no. 8, p. 1437, Aug. 2021.

[35] K. D. Tzimourta et al., "Analysis of electroencephalographic signals complexity regarding Alzheimer's disease," *Comput. Electr. Eng.*, vol. 76, pp. 198–212, Jun. 2019.

[36] H. Kamel, D. Abdulah, and J. M. Al-Tuwaijari, "Cancer classification using Gaussian Naive Bayes algorithm," in *Proc. Int. Eng. Conf. (IEC)*, Jun. 2019, pp. 165–170.

[37] K. Maswadi, N. A. Ghani, S. Hamid, and M. B. Rasheed, "Human activity classification using decision tree and Naïve Bayes classifiers," *Multimedia Tools Appl.*, vol. 80, no. 14, pp. 21709–21726, Jun. 2021.

[38] H. Hikawa, "Frequency-based multilayer neural network with on-chip learning and enhanced neuron characteristics," *IEEE Trans. Neural Netw.*, vol. 10, no. 3, pp. 545–553, May 1999.

[39] P. Xu et al., "Differentiating between psychogenic nonepileptic seizures and epilepsy based on common spatial pattern of weighted EEG resting networks," *IEEE Trans. Biomed. Eng.*, vol. 61, no. 6, pp. 1747–1755, Jun. 2014.

[40] C. Li et al., "Effective emotion recognition by learning discriminative graph topologies in EEG brain networks," *IEEE Trans. Neural Netw. Learn. Syst.*, early access, Feb. 2, 2023, doi: 10.1109/TNNLS.2023.3238519.

[41] L. Jiang et al., "Transcriptomic and macroscopic architectures of multimodal covariance network reveal molecular–structural–functional co-alterations," *Research*, vol. 6, p. 0171, Jan. 2023.